Atmospheric Energy Budgets in the Japanese Reanalysis: Evaluation and Variability

Kevin E. TRENBERTH and Lesley SMITH

National Center for Atmospheric Research[1]*, Boulder, Colorado, USA*

(*Manuscript received 10 March 2007, in final form 13 May 2008*)

Abstract

The vertically-integrated atmospheric energy and moisture budgets have been computed for all available months for the Japanese reanalysis (1979 to 2004), and results are described in detail for the month of January 1989 and compared with those of other reanalyses. Time series are also presented. The moistening, diabatic heating and total energy forcing of the atmosphere are computed as a residual from the analyses using the moisture, dry energy (dry static energy plus kinetic energy) and total atmospheric (moist static plus kinetic) energy budget equations. These fields are also computed from the model output based on the assimilating model parameterizations. Moreover, some component fields can also be computed from observations to evaluate the results. In particular, when the vertically-integrated forcings computed from the model parameterizations are compared with available observations and the budget-derived values, significant JRA model biases are revealed in radiation and precipitation. The energy and moisture budget-derived quantities are more realistic than the model output and better depict the real atmosphere. However, low frequency decadal variability is spurious and is mainly associated with changes in the observing system. Results also depend on the quality of the analyses which are not constructed to conserve mass, moisture or energy, owing to analysis increments. Although there has been considerable progress in depicting the diabatic components of the atmosphere, some problems remain, and suggestions are made on where research can make further improvements.

1. Introduction

A continuing interest is to document the flow of energy through the climate system for the annual mean, its annual cycle and its variability. The main focus of our work has been on the bulk vertically-integrated atmospheric energy budget (Trenberth et al. 2001; Trenberth and Stepaniak 2003a, b, 2004) and especially the role of water (Trenberth et al. 2007). The main datasets required are the full atmospheric analyses of all the state variables every 6 hours to enable the computation of various energy forms (internal energy, sensible heat, latent energy, potential energy, dry static energy, moist static energy, and kinetic energy), the storage and changes in storage (tendency) of these components, and their transports and divergences. In the past we have made extensive use of reanalyses from National Centers for Environmental Prediction/National Center for Atmospheric Research (NCEP/NCAR) (referred to as NRA) (Kalnay et al. 1996) and the European Centre for Medium Range Weather Forecasts (ECMWF), known as ERA-40 (Uppala et al. 2005). In this paper we report on results for the recent Japanese Reanalysis (JRA) (Onogi et al. 2007) starting in 1979.

Use is made of top-of-atmosphere (TOA) observed radiative fluxes from satellite measurements and computed surface fluxes into land or ocean to evaluate how well the energy budget can

Corresponding author: Kevin E. Trenberth, National Center for Atmospheric Research, P.O.Box 3000, Boulder, CO 80307, USA
E-mail: trenbert@ucar.edu

1 The National Center for Atmospheric Research is sponsored by the National Science Foundation.

be closed. Several recent studies have deduced the ocean heat storage and transports as a residual of the energy budget (Fasullo and Trenberth 2008a, b; Trenberth and Fasullo 2008) based on estimates of the surface heat fluxes (Trenberth et al. 2001), and compared results with ocean data to obtain a more holistic view of the energy flows and their uncertainties.

In the current study, we report on the analysis of the atmospheric energetics and heat budget from JRA and their comparison to observational constraints, with a primary focus on one month, January 1989, in detail as a follow on to two studies which used the same month to document computational issues for the vertically-integrated (Trenberth et al. 2002a) and full three dimensional (Trenberth and Smith 2008) energy quantities using other reanalyses. The mean annual cycle and monthly anomaly time series are also examined and compared with those of other reanalyses to determine reproducibility and credibility of results.

The energy and heat budget equations can be vertically integrated analytically and the results computed directly. The most accurate computations are possible in the model coordinates of the numerical weather prediction model used for data assimilation, and this is what is done here. Several respects of these computations are extremely demanding and are not straightforward. A prerequisite for determining the energy budget and energy transports is to have a balanced closed mass budget. Otherwise, there is an implied return flow, mandated by continuity, somewhere else that is transporting energy. Hence, for budget computation of any quantity, it is essential to also examine and balance the dry air mass budget (Trenberth 1991, 1997) and substantial adjustments are required to the energy terms to obtain sensible results. Although tendency terms are small for long-term averages, this is not the case for individual months (Trenberth et al. 2002a) and so they too have been computed.

Section 2 discusses the data used and the physical background and mathematical expressions for the energy and moisture budgets and their breakdown into components. Section 3 presents results for the month of January 1989. It also presents results of comparisons with observations and comparisons among the mean annual cycle and the time series variability for the 3 main reanalyses. The conclusions are given in Section 4.

2. Vertically-integrated moisture and energy budgets

The data used are from the JRA (Onogi et al. 2007). The full resolution four-times daily data on model coordinates have been used to obtain the best accuracy possible for the vertical integrals. JRA reanalyses have a horizontal resolution of T-106 and 40 levels in the vertical. The overall framework of the heat and moisture budgets was originally described by Yanai et al. (1973), although with equations that were not quite correct.

The thermodynamic equation, can be written in advective form as

$$c_P\left[\frac{\partial}{\partial t}T+\mathbf{v}.\nabla T+\omega\left(\frac{\partial}{\partial p}T-\kappa\frac{T}{p}\right)\right]=Q_1 \qquad (1)$$

where Q_1 is the diabatic heating per unit mass, T is temperature, $\mathbf{v}$ is the horizontal velocity, ω is the vertical p-velocity, and $\kappa = R/c_p$ and c_p is the specific heat at constant pressure. Adding in the kinetic energy equation to (1) gives the total dry energy equation

$$\frac{\partial}{\partial t}(c_pT+k)+\mathbf{v}.\nabla(s+k)+\omega\frac{\partial}{\partial p}(s+k)=Q_1-Q_f \quad (2a)$$

or in flux form

$$\frac{\partial}{\partial t}(c_pT+k)+\nabla\cdot(s+k)\mathbf{v}+\frac{\partial}{\partial p}(s+k)\omega=Q_1-Q_f \quad (2b)$$

where Q_f is the frictional heating arising from dissipation of kinetic energy, k is the kinetic energy, and $s = c_pT + \Phi$ is the dry static energy.

The potential advantage of this form is that it avoids the difficulties associated with the static stability term in the thermodynamic equation that is related to the conversion of potential and internal energy into kinetic energy, and which is sensitive to small errors. The flux form (2b) involves convergence or divergence of $s + k$, and has advantages because vertical differencing automatically cancels out terms and the vertical integral is easily computed. However, it requires very strict adherence to the equation of continuity being exactly satisfied. To ensure that the mass budget is balanced, we employ a barotropic correction to the divergent wind component (Trenberth 1991). Then ω can be computed by integrating from ei-

ther the bottom or the top of the atmosphere to the level of concern.

Vertically integrating (2b) gives

$$\frac{\partial}{\partial t}\frac{1}{g}\int_0^{p_s}(c_pT+k+\Phi_s)dp+\nabla.\frac{1}{g}\int_0^{p_s}(s+k)\mathbf{v}\,dp = \hat{Q}_1-\hat{Q}_f \quad (3)$$

where lower boundary conditions are fully accounted analytically and the ^ is the vertical integral.

We also use the conservation of moisture equation in advective form

$$\frac{\partial q}{\partial t}+\mathbf{v}.\nabla q+\omega\frac{\partial q}{\partial p}=e-c \quad (4)$$

where q is the specific humidity, e is the evaporation and c the condensation. When vertically integrated in flux form, this becomes

$$\frac{\partial}{\partial t}\frac{1}{g}\int_0^{p_s}q\,dp+\nabla.\frac{1}{g}\int_0^{p_s}\mathbf{v}q\,dp=E-P \quad (5)$$

where E is the surface evaporation and P is the net surface precipitation rate. The whole equation can be expressed also in terms of energy by multiplying by L, the latent heat of vaporization. Frequently the term $\hat{Q}_2=L(P-E)$ is referred to as the apparent latent heating arising from the apparent moistening (see Trenberth (1997) for more details). The use of "apparent" here is because it includes all the small scale unresolved eddy effects as well. When (5) in energy form is added to (3), the equation becomes the equation for the transport of moist static energy $h = s + Lq$ plus kinetic energy k, although the evolution is of the total atmospheric energy $AE = c_pT + \Phi_s + k + Lq$ where Φ_s is the surface geopotential.

$$\frac{\partial}{\partial t}\frac{1}{g}\int_0^{p_s}(c_pT+k+\Phi_s+Lq)dq+\nabla.\frac{1}{g}\int_0^{p_s}(h+k)\mathbf{v}dp = \hat{Q}_1-\hat{Q}_f-\hat{Q}_2. \quad (6)$$

If we set $T=\overline{T}+T'$, where the overbar is the time average and the prime is the departure, and similarly for all of the other variables, then we can also compute mean and transient eddy flux terms.

The tendency terms are computed from the difference between the value at the end of the month minus that at the beginning of the month, interpolated to the correct time of 2100 UTC prior to the first analysis time of each month. However, the tendency terms are given in Trenberth et al. (2002a) and will not be presented here. The Q_1 and Q_2 terms are computed as residuals from the heat and moisture equations and include contributions from small-scale unresolved processes. Q_1 includes Q_f but the latter is very small (Li et al. 2007) and can be neglected for most purposes.

For the vertical integrals, $\hat{Q}_1$ is the sum of the downward net radiation at the TOA, the surface sensible and radiative heating and the latent heating plus any small scale effects. Consequently, $\hat{Q}_1 - \hat{Q}_2$ is the sum of the TOA downward radiation plus the net upward surface fluxes, including the evaporative moistening flux LE. Therefore it is also the net radiative flux convergence plus the sensible heating and latent energy moistening.

We can also compute the atmospheric forcing terms Q_1, Q_2 and $Q_1 - Q_2$ from model results. In the case of the JRA reanalyses, the vertical integrals can be computed as follows:

$$\hat{Q}_1 = R + SH + LP \quad (7)$$

$$\hat{Q}_2 = L(P - E) \quad (8)$$

$$\hat{Q}_1 - \hat{Q}_2 = R + SH + LE \quad (9)$$

where R is the net radiation convergence and is made up of the solar and long-wave components, and SH is the surface sensible heat. The archive has the surface sensible and latent heat fluxes as well as surface and TOA radiation in solar and thermal bands. These are accumulated fields based on the assimilating model parameterizations and physics, and have an advantage in that they do not suffer from temporal sampling, but the disadvantage in that they are not observed quantities. For JRA, L is a constant 2.507×10^6 J kg^{-1}.

3. Results

a. Vertical integrals for January 1989

Computational results for January 1989 of the vertically-integrated diabatic heating, Q_1, the latent energy from moistening $-Q_2$, and the total forcing $Q_1 - Q_2$ are shown in Fig. 1 using the exact vertical integral in full model coordinates. We interpret $Q_1 - Q_f$ for the most part as Q_1. Note that $-Q_2 = L(E - P)$ in W m^{-2} can be converted to give $E - P$ units of mm/day by dividing by a factor of 29. Zonal means are shown in the right panels and the plots are truncated to T42 resolution. The

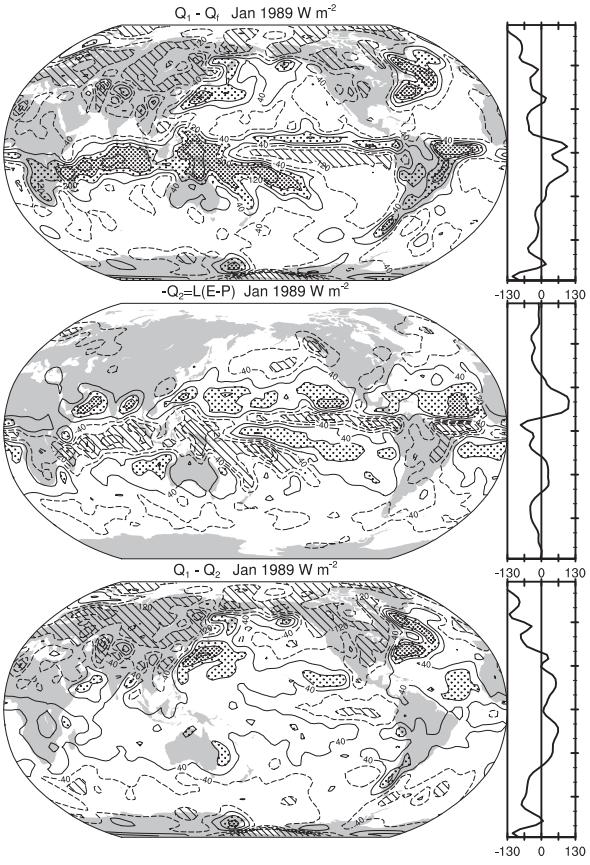

Fig. 1. For Jan 1989 based on JRA analyses, vertically integrated Q_1, $-Q_2$ and $Q_1 - Q_2$. The right hand side panels show the zonal averages. The plots are smoothed to T42 resolution and the units are W m^{-2}. Contour interval is 80 W m^{-2}, and stipple and hatching begin at ±120 W m^{-2} and more densely at ±200 W m^{-2}.

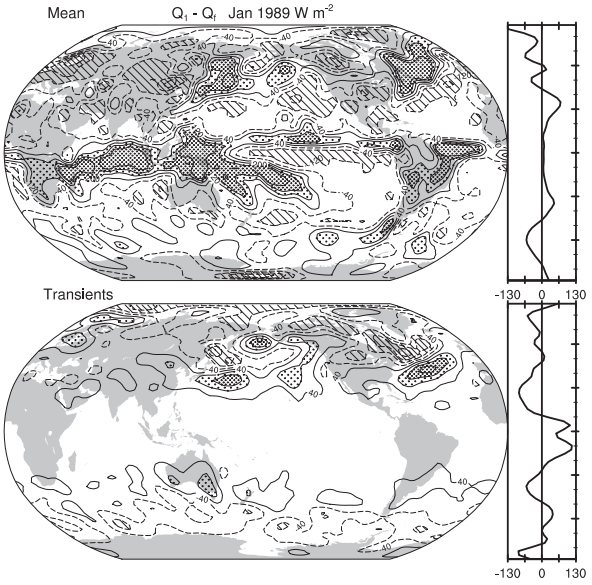

Fig. 2. Vertically integrated contributions to Q_1 from the mean terms (top), transient terms (bottom). The plots are smoothed to T42 resolution and the units are W m^{-2}. Contour interval is 80 W m^{-2}, and stipple and hatching begin at ±120 W m^{-2} and more densely at ±200 W m^{-2}.

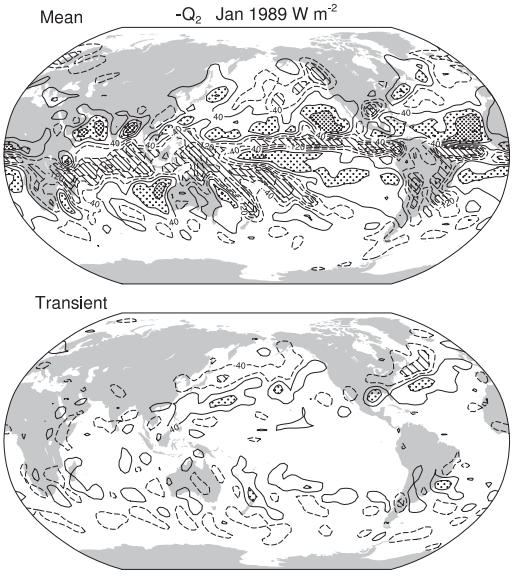

Fig. 3. Vertically integrated contributions to $-Q_2$ from the mean (top) and transients (bottom). The plots are smoothed to T42 resolution and the units are W m^{-2}. Contour interval is 80 W m^{-2}, and stipple and hatching begin at ±120 W m^{-2} and more densely at ±200 W m^{-2}.

tendency term for this month (not shown) contributes up to about 50 W m^{-2}, and is fairly small but not negligible.

The various terms, vertically integrated, that contribute to Q_1 (Fig. 2) reveal that the main contributions come from the monthly mean advection terms while the transients contribute most in the extratropics and, not unexpectedly, are strongest in the winter hemisphere over the oceans in association with the storm tracks. Examining the mean and transient contributions to the moisture fluxes that result in evaporation or precipitation shows that the mean terms also strongly dominate the transient terms (Fig. 3).

Interpretation of these figures is aided by recognizing the contributions to them as in (7), (8) and (9). Q_2 is simplest to interpret as it is dominated by precipitation patterns and reveals the Inter-Tropical Convergence Zone (ITCZ) over the Pacific, Atlantic and Indian Oceans, the South Pacific Convergence Zone (SPCZ), and the monsoon rains over South America, northern Australia and central Africa south of the equator. It also reveals the dominance of precipitation in the extratropical storm tracks over the oceans. In the subtropics, evaporation dominates in the subtropical high pressure regions over the oceans. Over land, it is expected that P > E as runoff is positive unless there are lakes and rivers present. Similarly, Q_1 is dominated in terms of the patterns by precipitation latent heat release. However, it also has a large radiative cooling component that is largest over the Arctic and northern continents in January. In the $Q_1 - Q_2$ panel, the precipitation component cancels and radiative cooling dominates in the extratropics while evaporative moistening dominates throughout much of the tropics and subtropics, even over land, with the notable exception of the equatorial cold tongue in the tropical Pacific. Some of the small-scale structure, notably the positive blobs over northern continents, is likely related to uncertainties in the analyses, as we shall see later (Fig. 4).

The strong cancellation between Q_1 and Q_2 (Fig.

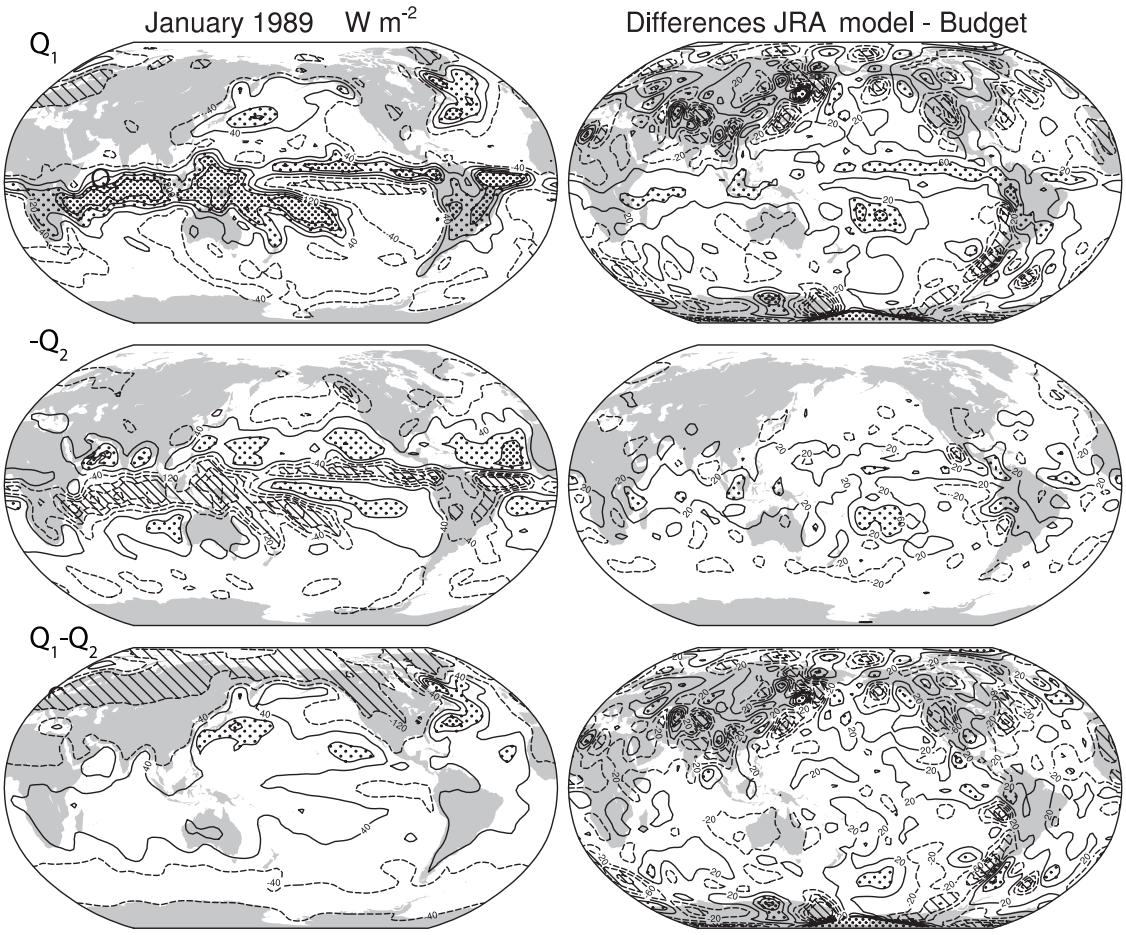

Fig. 4. Q_1, $-Q_2$ and $Q_1 - Q_2$ estimated directly from the model accumulated values and their differences with the vertically-integrated budget derived quantities in Fig. 1. The plots are smoothed to T42 resolution and the units are W m^{-2}. For the plots at left, the contour interval is 80 W m^{-2}, and stipple and hatching begin at ±120 W m^{-2} and more densely at ±200 W m^{-2}. For the difference plots at right, the contour interval is 40 W m^{-2}, and stipple and hatching begin at ±60 W m^{-2} and more densely at ±100 W m^{-2}.

1) occurs as latent heat is realized and converted to dry static energy. Hence their combination on the right hand side of (6), $Q_1 - Q_2$ (Fig. 1), has less structure as the computed forcing of the total energy mostly has the moistening of the atmosphere but no latent heat component. However, there is a residual of the precipitation patterns in the $Q_1 - Q_2$ map, partly reflecting the evaporative sources of moisture being dominant in tradewind domains, and presumably also indicating the related radiative effects from the distributions of cloud and water vapor associated with precipitation.

For comparison, Fig. 4 shows the result of direct computation of Q_1, Q_2 and $Q_1 - Q_2$ from the model parameterizations used in the reanalyses computed from (7), (8) and (9). Also shown are the differences from the budget quantities in Fig. 1. The fields are quite similar overall, although with much less small-scale structure over land, and also with some large-scale differences that are quite substantial. These can be traced for the most part to model biases and known problems with the JRA fields (Fig. 5); see the next section.

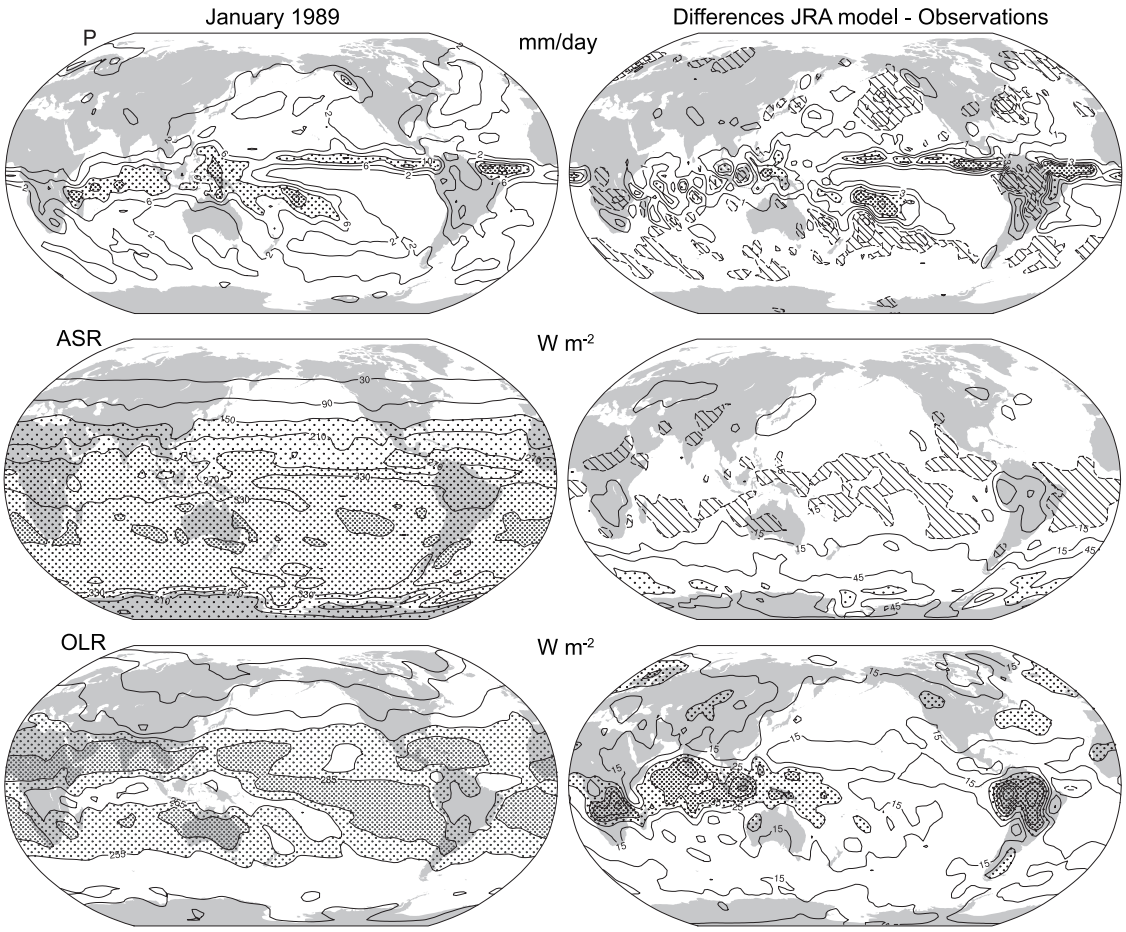

Fig. 5. Model based values (left) of precipitation P, ASR, and OLR, and the model values minus observed in W m^{-2} (right). For P contours are every 4 mm/day with stipple at 10 and 14 mm/day. For the P differences, the contour interval is 2 mm/day, hatching occurs at –3 and –1 mm/day and stipple at 5 and 7 mm/day. For ASR contours are every 60 W m^{-2} and stipple occurs for values greater than 150, 270 and 390 W m^{-2}. For ASR differences, contour interval is 30 W m^{-2} with hatching at –15 W m^{-2} and stipple at 75 W m^{-2}. For OLR contours are every 30 W m^{-2} and stipple begins at 255 and 285 W m^{-2}. For the OLR difference plot at right, the contour interval is 10 W m^{-2}, and stipple begins at 25 and 35 W m^{-2}.

b. Comparison with atmospheric forcings

Trenberth et al. (2008) has assessed the annual global mean energy budget for the ERBE and CERES periods based on observations and compared with reanalyses. For JRA in general for 1979 to 2004, the global planetary albedo is low by about 2% compared with CERES estimates, global absorbed solar radiation (ASR) is high by 5 W m^{-2}, and outgoing longwave radiation (OLR) is high by 15 W m^{-2}, so there is a global imbalance of 9.1 W m^{-2} upwards. In contrast the best estimate is a downward flux contributing to warming of 0.9 W m^{-2}. Accordingly, even though too much radiation is absorbed, the bias in OLR dominates. Global surface latent heating due to evaporation is 85.1 W m^{-2} for the ERBE period; about 9 W m^{-2} higher than observational estimates. These biases are also present in January 1989, as detailed below.

To help establish these aspects, we therefore present (Fig. 5) the precipitation from the model and differences from the Global Precipitation Climatology Project (GPCP) (Adler et al. 2003), and TOA radiation for the ASR and OLR components differenced with ERBE (Trenberth 1997).

There is an overestimate of tropical precipitation exceeding 7 mm/day in places which shows up as excess latent heating of 30 to > 120 W m^{-2} and with zonal average differences of 7 mm/day (203 W m^{-2}) at 7°N. There are also biases in location as the SPCZ is shifted north, leaving large negative biases, up to 7 mm/day (210 W m^{-2}), especially over the southwest Pacific, and zonal mean negative biases of –26 W m^{-2} at 40°S. Comparable negative biases exist regionally in the northern extratropics. Globally the bias in precipitation in model values is 0.46 mm/day (13.4 W m^{-2}) compared with the global mean of 2.71 mm/day (78.5 W m^{-2}).

Although much of the bias in Q_2 (Fig. 4) is traceable to the precipitation field, the pattern is not the same as the precipitation bias (Fig. 5) and so one interpretation is that evaporation biases also exist. As the model Q_2 has a global mean of 6.7 W m^{-2} whereas the tendency in moisture storage is 0.02 W m^{-2}, the model value is biased high by 6.7 W m^{-2}. This also implies that the global mean model *LE* of 86.5 W m^{-2} for January 1989 is biased high by 6.7 W m^{-2} to the extent that the model *LP* is compatible with the budget inferred Q_2. This is reasonable, given that the model *LE* exceeds *LP* from GPCP by 8 W m^{-2}. That in turn suggests that the hydrological cycle is much too active in the JRA model and that the excess of *P* over *E* comes from analysis increments that moisten the atmosphere to compensate for the excessive rains. Hence much of the differences in estimates of Q_2 (Fig. 4) are accounted for as model bias.

Substantial biases also exist in radiation fields (Fig. 5). The OLR (directed up) is too large in the JRA model almost everywhere and especially in deep convections regions over the tropical Indian Ocean and African and South American monsoon regions, with biases of 5 to 50 W m^{-2}. This suggests that cloud is too low or has the wrong radiative properties. On the other hand, the ASR biases are negative in the tropics and subtropics suggesting that the surface or cloud is too bright. Given that it is pervasive except in areas of stratocumulus cloud, which are reasonably well simulated (Onogi et al. 2007) and the bias includes relatively cloud free areas, it may relate to the finding of Onogi et al. (2007) that the planetary albedo is too high in the radiation scheme used in JRA, and this has since been corrected in the model but not in time for JRA. However, the positive bias of 10 to well over 70 W m^{-2} over the southern oceans is suggestive of not enough cloud, a common error in climate models.

The observed tendency in global mean Q_1 is –0.1 W m^{-2}, while the global model Q_1 is 7.2 W m^{-2} in spite of a 13.4 W m^{-2} bias contribution from latent heat. These suggest that the sum of the global means of sensible heat of 17.0 W m^{-2} plus radiation of –103.0 W m^{-2} are biased by –6.1 W m^{-2}, and so this emphasizes the negative bias in radiative cooling. This value is compatible with the direct comparisons for ASR and OLR; global mean ASR is too high by 13.0 W m^{-2} and OLR is too high by 19.6 W m^{-2} for January 1989 based on the ERBE results. Indeed for $Q_1 - Q_2$, coming from the sum of radiation and surface fluxes of sensible and evaporative latent heat, the global mean bias is only 0.6 W m^{-2} so the evaporation and radiation biases largely cancel.

Hence much of the large-scale structure in the difference panels of Fig. 4 can be traced to model biases. The small-scale structure, which clearly originates from the budget calculations, relates to the divergence term. The differences of the model precipitation with observations are quite similar to those for ERA-40 for January 1989 (Trenberth and Smith 2008). However, the radiation biases

are rather different and larger for JRA.

c. Mean annual cycle

The mean annual cycle of the zonal mean divergence of vertically integrated dry static energy, latent energy and total atmospheric energy is given in Fig. 6 for JRA from 1979 to 2004. The latent energy divergence patterns are dominated by the tropics and relate to the annual cycle of the ITCZ and associated monsoon troughs. In northern summer, values are strongest negative near 10 °N as the ITCZ and the monsoons rains reinforce each other in the zonal mean, while in January, the increased activity in the SPCZ is blurred out in the zonal means although negative values occur south of the equator. Also in January, the 5 to 10 °N values are much weaker as the winter northern monsoon partly cancels the ocean ITCZ rains in the zonal mean. The dominance of strong subtropical evaporation in the winter half year is also evident in Fig. 6 for latent energy divergence. The precipitation signature is reversed in sign in the dry static energy divergence, but elsewhere radiative cooling also enters, notably at high latitudes and in the dry subtropical high regions. Hence for the total energy divergence, the moistening in the subtropics provides for order 50 W m^{-2} that compensates for the radiative losses at high latitudes, where values are much larger in magnitude (< −100 W m^{-2}) owing to the smaller area from convergence of the meridians.

Maps of the divergence of dry static energy (DSE) and latent energy (LE) from JRA and differences with the corresponding fields from NRA and ERA-40 are given in Fig. 7. This figure reveals the spatial structure of the zonal mean features of Fig. 6. It also shows that the biggest differences with other reanalyses arise in the tropics in association with the main precipitation areas. Some large differences are also evident over Antarctica and other regions (Himalayas, Andes, and Greenland) where high topography plays a role.

d. Variability

Figure 8 shows the zonal mean latitude-time series of the monthly anomalies of divergence of the total atmospheric energy, DSE and LE. A similar plot for NRA results is given in Trenberth et al. (2002b). In Fig. 8 the values have been filtered with the 13 point low pass filter (Trenberth et al. 2007) designed to reveal annual variations and longer. It highlights the significant variability in both the DSE and LE and with a strong negative correlation (Fig. 9) in monthly mean values especially in the tropics. This negative relation is the manifestation of the release of latent heat showing up as an increase in dry static energy. The strongest features revealed in Fig. 8 are the 1982–83 and 1997–98 El Niño events. In 1982–83 anomalies exceed 20 W m^{-2} in both LE and DSE divergence, while in 1997–98 anomalies exceed 50 W m^{-2}. In both cases there are strong dipoles signifying shifts in patterns and fairly local compensation. Yet for the total energy divergence, the

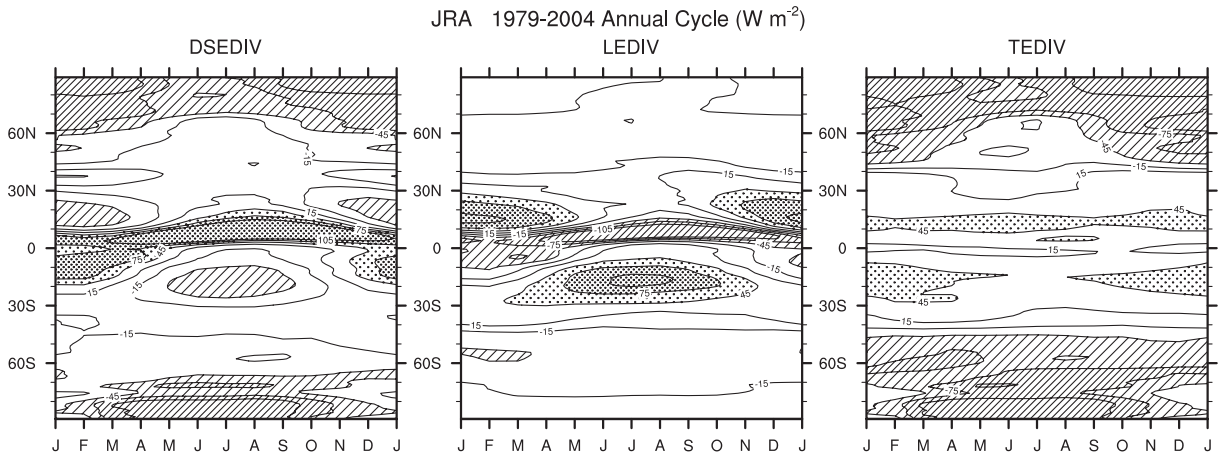

Fig. 6. Latitude-time series of zonal mean divergence of DSE, LE and total atmospheric energy for 1979 to 2004 in W m^{-2} for the mean annual cycle. The contour interval is 30 W m^{-2} and stipple or hatching begins at ±45 and ±75 W m^{-2} (denser).

associated residuals are less than about 10 W m^{-2}. The overall size of the anomalies can be seen from the standard deviation of the monthly zonal mean values given at the bottom of Fig. 8. Many aspects of the interannual variability in Fig. 8 are similar to those for NRA in Trenberth et al. (2002b). However, dominant features of Fig. 8 are the low frequency nonlinear trends that turn out unfortunately to be spurious. These are pronounced but equal and opposite at about 10 to 15°N vs 10–15 °S for both DSE and LE, and they leave a residual for the total energy divergence.

Correlation maps of these monthly anomaly fields between different reanalyses (Fig. 10) show the poor correlations and large discrepancies with other reanalyses in regions of convection and strong divergent flow throughout the tropics. Over the oceans outside of the tropics, the correlations exceed about 0.7.

Time series at 14°N and 62°N highlight the differences among the three analyses. For the total energy divergence at 14°N (Fig. 11), time series reveal a big drop in JRA in late 1988, a large jump in ERA-40 about 1992, and little variability in NRA. The problems in ERA-40, especially associated with the Mount Pinatubo eruption aerosol effects developing in 1991, are well established (Uppala et al. 2005). SSM/I data were assimilated only by JRA and ERA-40, which likely contributes to some differences with NRA beginning in mid-1987. The deficiencies of variability in NRA are also well established over the oceans where SSM/I data were not assimilated and water vapor variability is too small and has incorrect structure (Trenberth et al. 2005). The drop in JRA (Fig. 11) in late 1988 coincides with the loss

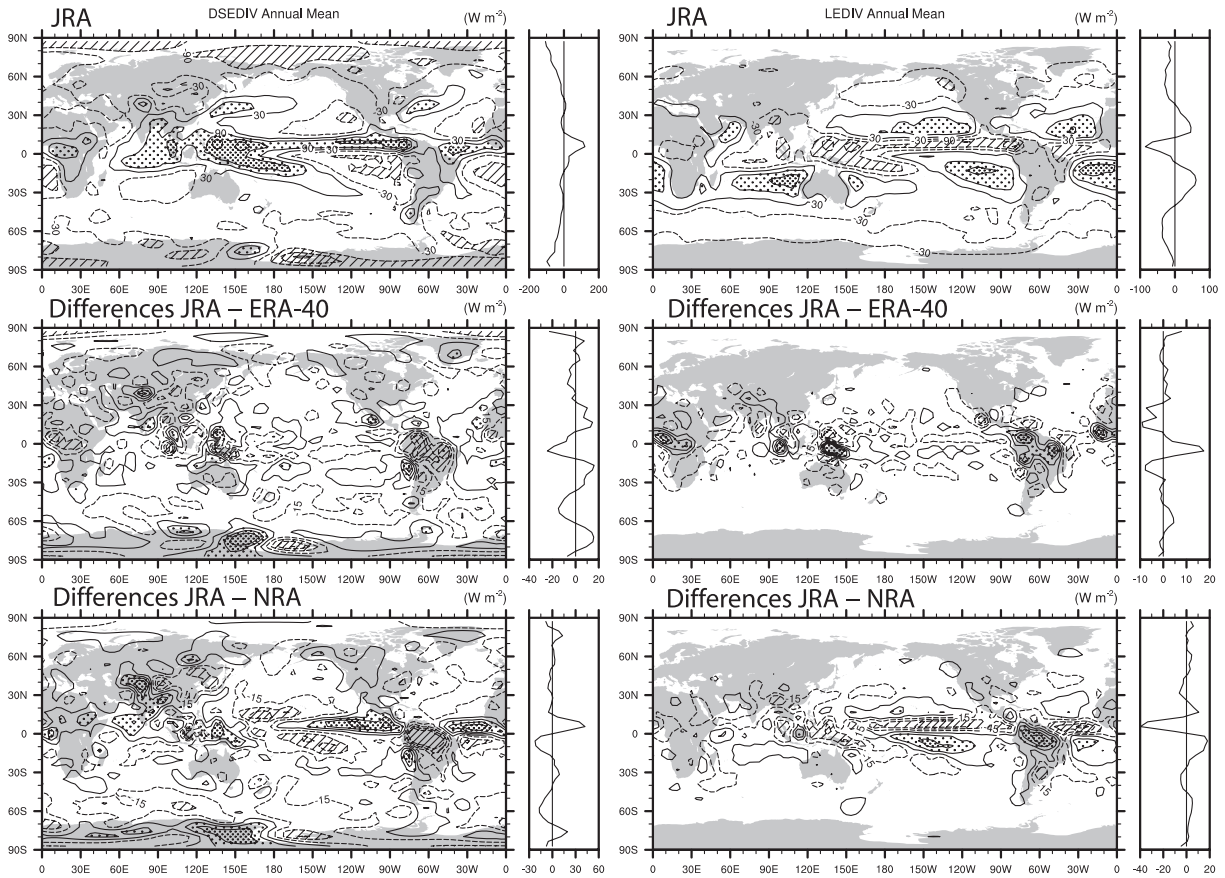

Fig. 7. Annual mean 1979–2001 vertically integrated DSE and LE divergence. The top panel gives values from JRA and the lower panels give differences from ERA-40 and NRA. In the top panel the contour interval is 60 W m^{-2} and values are stippled or hatched at ±90 and ±150 W m^{-2}, while contours and shading are halved in the lower two panels. Negative contours are dashed.

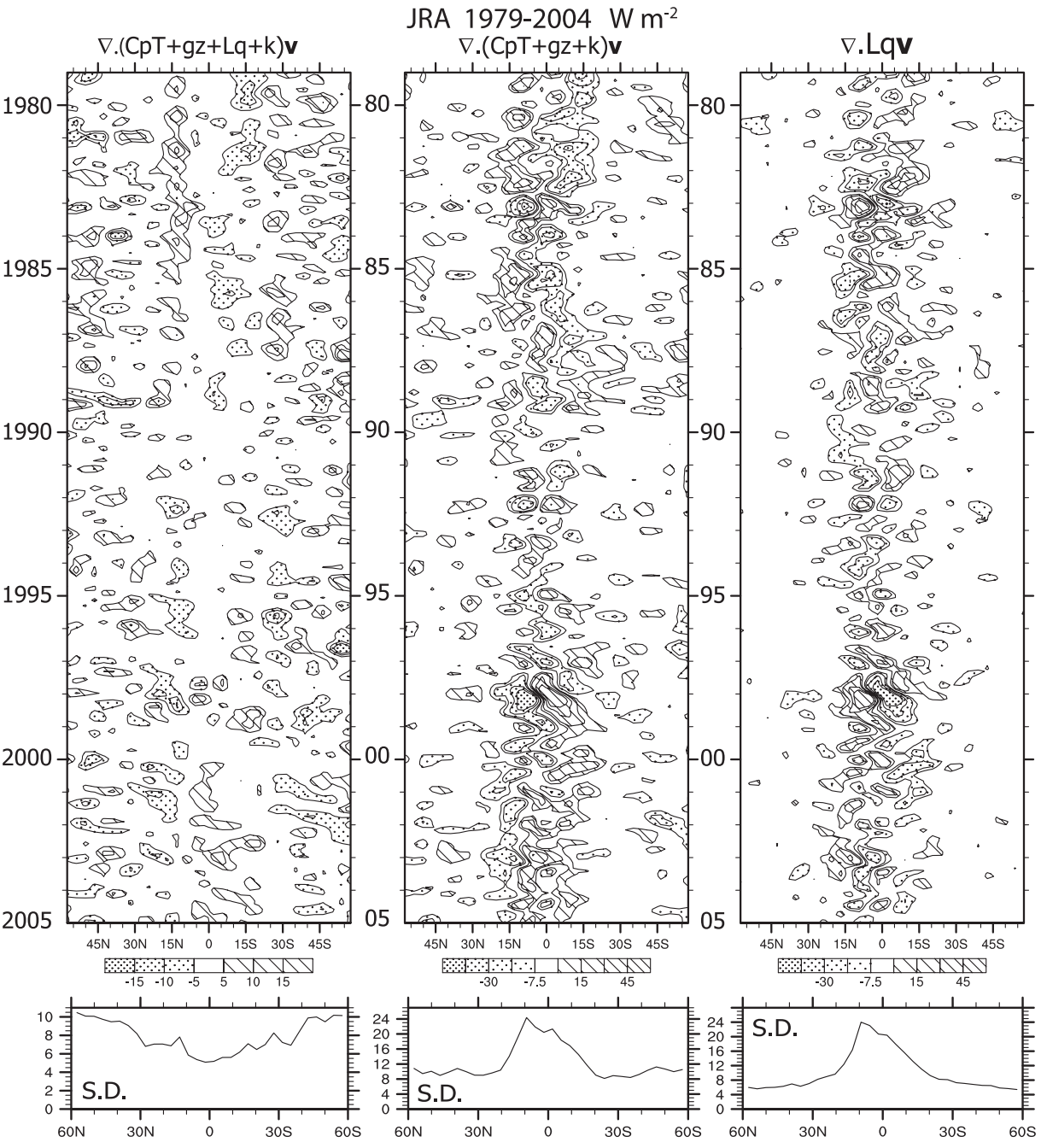

Fig. 8. Latitude-time series of zonal monthly mean anomalies of divergence of total energy, DSE, and LE, for 1979 to 2004 in W m^{-2}. Values have been smoothed with a 13 point filter to show interannual variations. The contour interval is 15 W m^{-2} in the middle and right panels and 10 W m^{-2} in the left panel. Below, the standard deviation of the monthly anomalies is given.

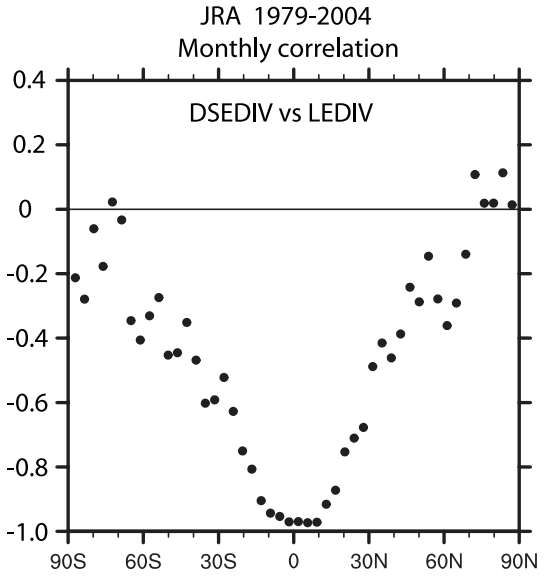

of NOAA-9 and start of NOAA-11 soundings. This affected all reanalyses in different ways, and so it is less apparent in the difference time series than in the JRA field by itself. In general, the month to month variations are well reproduced, but the decadal and longer term variability is completely different among all three reanalyses.

These differences extend well outside the tropics, as seen from time series at 62°N (Fig. 12). Once again the decadal variability is large in JRA

Fig. 9. Correlation between monthly zonal mean anomalies of divergence of DSE vs LE for 1979 to 2004 (312 months). Values exceeding 0.12 in magnitude are statistically significant at the 5% level.

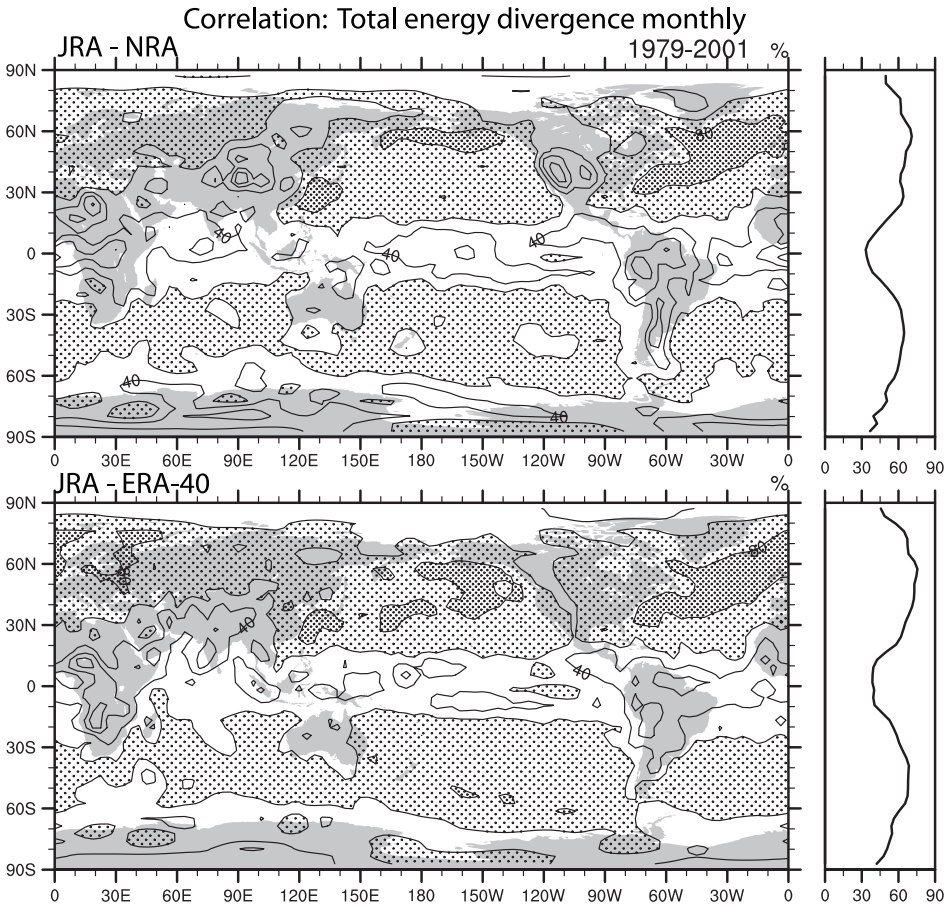

Fig. 10. Correlations of monthly anomalies in total atmospheric energy divergence of JRA with NRA (top) and JRA with ERA-40 (bottom) at T31 resolution for 1979 to 2001. The contour interval is 20% and values exceeding 60% are coarse stippled and 80% fine stippled.

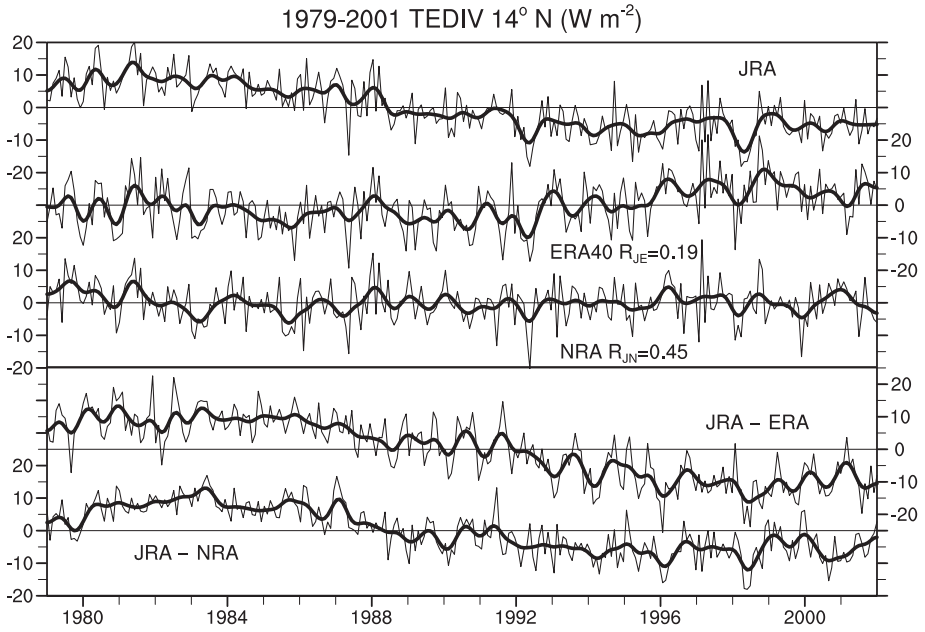

Fig. 11. Time series of the monthly anomalies of the zonal mean divergence of the column integrated total atmospheric energy at 14°N from JRA (top), ERA-40 (top middle) and NRA (top lower) in W m^{-2}. The correlation between JRA and ERA-40 and NRA are given on the plot. The bottom panel shows the differences between JRA and ERA-40, and JRA and NRA. The heavy line is a 13–term filter to show the interannual variations.

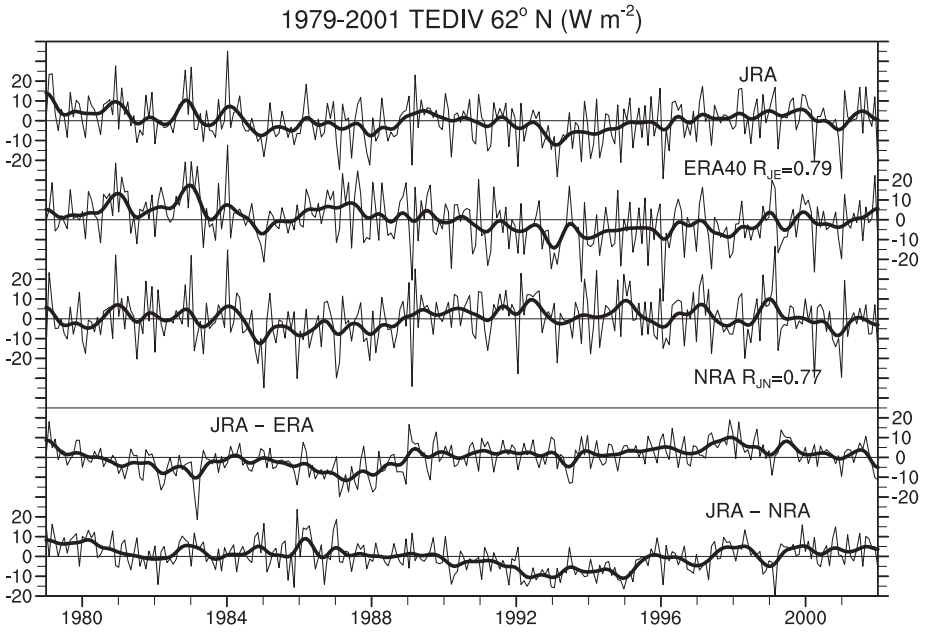

Fig. 12. Time series of the monthly anomalies of the zonal mean divergence of the column integrated total atmospheric energy at 62°N from JRA (top), ERA-40 (top middle) and NRA (top lower) in W m^{-2}. The correlation between JRA and ERA-40 and NRA are given on the plot. The bottom panel shows the differences between JRA and ERA-40, and JRA and NRA. The heavy line is a 13–term filter to show the interannual variations.

and ERA-40 but quite different, and both differ from NRA. Yet the monthly correlations are 0.79 for JRA with ERA-40 and 0.77 for JRA with NRA, highlighting the very good agreement from month to month even as there is poor agreement at low frequencies. Once again, the late 1988 date shows up in the differences with ERA-40, although NRA differences emerge more about 1990, perhaps in association with the end of one stream and beginning of another stream of the JRA reanalyses (Onogi et al. 2007).

4. Discussion and conclusions

In this paper, we document an approach to diagnosing the moistening and diabatic heating of the atmosphere based upon the dry energy and moisture equations and their combination for the total energy. The main focus was on a detailed documentation of January 1989 when ERBE data exist to help validate the results. Brief results for other months are presented as well.

In general there is good fidelity of the synoptic features in the extratropics and agreement in the overall energy quantities among the reanalyses. However, the low frequency variability has no resemblance among the reanalyses and none of them are considered realistic. Problems are especially evident in areas where precipitation occurs. NRA features unrealistic trends and variability is too low over the oceans, as information from water vapor channels were not assimilated (Trenberth et al. 2005). In ERA-40 and JRA, spurious variability is readily identified and is associated with changes in the observing system or inability to properly handle some forcings, namely the effect of Pinatubo aerosols on radiances. Bias corrections across changing satellite platforms and instruments are an outstanding issue based on these reanalyses.

An analysis of some atmospheric forcings or variables (precipitation) for January 1989 as computed from the assimilating JRA model reveals significant biases when compared with observations and these biases are reflected in the differences computed with the budget-derived quantities, suggesting that the latter are considerably more reliable. However, only their sum can be computed from the energy and moisture budgets and the model-derived fields can provide extra information to aid in interpretation. Nonetheless, comparing the budget-derived results with the model parameterizations then provides a useful tool for determining model biases.

For the JRA model, biases in albedo and clouds affect the radiation. Precipitation biases are similar to but not identical to those for ERA-40 for January 1989, highlighting the difficulty in reproducing the ITCZ and SPCZ. The mean differences among the 3 reanalyses and also the time series of the energy quantities reveal poor reproducibility in all areas of rainfall throughout the tropics: the ITCZ, the SPCZ and the monsoon troughs. Hence the divergent part of the atmospheric circulation is not well reproduced. This is known to be not well constrained by observations that are assimilated. Hence cloud and precipitation remain important fields for validating models and reanalyses.

By emphasizing the differences and the errors in the above, there is a tendency to overlook the fact that the overall fields among reanalyses are quite similar, and even though they are not perfect, this is a considerable advance over just a few years ago. In other words, these results highlight considerable progress, but also point to where research could make further improvements.

The JRA reanalysis is a valuable addition to the information about past climate as it provides a different perspective than previous reanalyses with different strengths and limitations. It is evident that global atmospheric reanalyses result in high-quality and consistent estimates of the short-term or synoptic-scale variations of the atmosphere, but variability on longer time scales (especially decadal) is not so well captured – at least yet. The primary causes of this deficiency are the quality and homogeneity of the fundamental data sets that make up the climate record and the quality of the data assimilation systems used to produce reanalyses. However, research into bias corrections and advanced reanalysis techniques is showing promise, and further reanalysis efforts are needed.

Acknowledgements

This research is partially sponsored by the NOAA CCDD and CLIVAR programs under grants NA07OAR4310051 and NA06OAR4310145.

References

Adler, R.F., G.J. Huffman, A. Chang, R. Ferraro, P. Xie, J. Janowiak, B. Rudolf, U. Schneider, S. Curtis, D. Bolvin, A. Gruber, J. Susskind, P. Arkin, and E. Nelkin, 2003: The version 2 Global Precipitation

Climatology Project (GPCP) monthly precipitation analysis (1979-present). *J. Hydrometeor.*, **4**, 1147–1167.

Fasullo, J.T. and K.E. Trenberth, 2008a: The annual cycle of the energy budget: Pt. I: Global mean and land-ocean exchanges. *J. Climate*, **21**, 2297–2313.

Fasullo, J.T. and K.E. Trenberth, 2008b: The annual cycle of the energy budget: Pt II: Meridional structures and poleward transports. *J. Climate*, **21**, 2314–2326.

IPCC, 2007: *Climate Change 2007. The Physical Science Basis*. Contribution of WG 1 to the Fourth Assessment Report of the Intergovernmental Panel on Climate Change. [S. Solomon, D. Qin, M. Manning, Z. Chen, M.C. Marquis, K.B. Averyt, M. Tignor, and H.L. Miller (eds)]. Cambridge University Press. Cambridge, U.K., and New York, NY, USA, 996 pp.

Kalnay, E., M. Kanamitsu, R. Kistler, W. Collins, D. Deaven, L. Gandin, M. Iredell, S. Saha, G. White, J. Woollen, Y. Zhu, A. Leetmaa, B. Reynolds, M. Chelliah, W. Ebisuzaki, W. Higgins, J. Janowiak, K.C. Mo, C. Ropelewski, J. Wang, R. Jenne, and D. Joseph, 1996: The NCEP/NCAR 40-Year Reanalysis Project. *Bull. Amer. Meteorol. Soc.*, **77**, 437–471.

Li L., A.P. Ingersoll, X. Jiang, D. Feldman, and Y. Yung 2007: Lorenz energy cycle of the global atmosphere based on reanalysis datasets. *Geophys. Res. Lett.*, **34**, L16813, Doi 10.1029/2007GL029985

Onogi, K., J. Tsutsui, H. Koide, M. Sakamoto, S. Kobayashi, H. Hatsushika, T. Matsumoto, N. Yamazaki, H. Kamahori, K. Takahashi, S. Kadokura, K. Wada, K. Kato, R. Oyama, T. Ose, N. Mannoji, and R. Taira, 2007: The JRA-25 Reanalysis. *J. Meteor. Soc.* Japan, **85**, 369–432.

Trenberth, K.E., 1991: Climate diagnostics from global analyses: Conservation of mass in ECMWF analyses. *J. Climate*, **4**, 707–722.

Trenberth, K.E., 1997: Using atmospheric budgets as a constraint on surface fluxes. *J. Climate*, **10**, 2796–2809.

Trenberth, K.E. and J. Fasullo, 2008: An observational estimate of ocean energy divergence. *J. Phys. Oceanogr.*, **38**, 984–999.

Trenberth, K.E. and L. Smith 2008: The three dimensional structure of the atmospheric energy budget: methodology and evaluation. *Clim. Dyn.*, doi 10.107/s00382-008-0389-3, in press

Trenberth, K.E. and D.P. Stepaniak, 2003a: Co-variability of components of poleward atmospheric energy transports on seasonal and interannual timescales. *J. Climate*, **16**, 3691–3705

Trenberth, K.E. and D.P. Stepaniak, 2003b: Seamless poleward atmospheric energy transports and implications for the Hadley circulation. *J. Climate*, **16**, 3706–3722.

Trenberth, K.E. and D.P. Stepaniak, 2004: The flow of energy through the Earth's climate system. 2004. *Quart. J. Roy. Meteor. Soc.*, **130**, 2677–2701.

Trenberth, K.E., J.T. Fasullo, and J. Kiehl, 2008: Earth's global energy budget. *Bull. Amer. Meteor. Soc.*, submitted.

Trenberth, K.E., J.M. Caron, and D.P. Stepaniak, 2001: The atmospheric energy budget and implications for surface fluxes and ocean heat transports. *Clim. Dyn.*, **17**, 259–276.

Trenberth, K.E., D.P. Stepaniak, and J.M. Caron, 2002a: Accuracy of atmospheric energy budgets. *J. Climate*, **15**, 3343–3360.

Trenberth, K.E., D.P. Stepaniak, and J.M. Caron 2002b: Interannual variations in the atmospheric heat budget. *J. Geophys. Res.*, **107**, D8, 10.1029/2000JD000297.

Trenberth, K.E., J. Fasullo, and L. Smith, 2005: Trends and variability in column-integrated water vapor. *Clim. Dyn.*, **24**, 741–758.

Trenberth, K.E., L. Smith, T. Qian, A. Dai, and J. Fasullo, 2007: Estimates of the global water budget and its annual cycle using observational and model data. *J. Hydrometeor.*, **8**, 758–769.

Uppala, S.M. et al., 2005: The ERA-40 reanalysis. *Quart. J. Roy. Meteor. Soc.*, **131**, 2961–3012.

Yanai, M., S. Esbensen, and J.H. Chu, 1973: Determination of bulk properties of tropical cloud clusters from large-scale heat and moisture budgets. *J. Atmos. Sci.*, **30**, 611–627.